Experimental Neurology 318 (2019) 61–70

Contents lists available at ScienceDirect

Experimental Neurology

journal homepage: www.elsevier.com/locate/yexnr

Research paper

Gnal haploinsufficiency causes genomic instability and increased sensitivity to haloperidol

Mohammad Moshahid Khan[a,b,c,*], Jianfeng Xiao[a,c], T.J. Hollingsworth[c], Damini Patel[a], Dana E. Selley[d], Trevor L. Ring[a], Mark S. LeDoux[e,**]

[a] Department of Neurology, University of Tennessee Health Science Center, Memphis, TN 38163, USA
[b] Division of Rehabilitation Sciences, Department of Physical Therapy, College of Health Professions, University of Tennessee Health Science Center, Memphis, TN, USA
[c] Neuroscience Institute, University of Tennessee Health Science Center, Memphis, TN 38163, USA
[d] Department of Pharmacology and Toxicology, Virginia Commonwealth University, Richmond, VA 23298, USA
[e] Department of Psychology, University of Memphis, Memphis, TN 38152, USA

ARTICLE INFO

Keywords:
Dystonia
Gα(olf)
Haloperidol
Striatum
DNA methylation
Dopamine receptor
Histone
Catalepsy

ABSTRACT

GNAL encodes guanine nucleotide-binding protein subunit Gα(olf) which plays a key role in striatal medium spiny neuron (MSN)-dopamine signaling. *GNAL* loss-of-function mutations are causally-associated with isolated dystonia, a movement disorder characterized by involuntary muscle contractions leading to abnormal postures. Dopamine D2 receptor (D2R) blockers such as haloperidol are mainstays in the treatment of psychosis but may contribute to the development of secondary acute and tardive dystonia. Administration of haloperidol promotes cAMP-dependent signaling in D2R-expressing indirect pathway MSNs. At present, little is known about the cellular relationships among isolated, acute, and tardive dystonia. Herein, we report the effects of acute D2R blockade on motor behavior, DNA repair, cAMP-mediated histone H3 phosphorylation (Ser10), and cell death in *Gnal*$^{+/-}$ mice and their isogenic *Gnal*$^{+/+}$ littermates. In comparison to *Gnal*$^{+/+}$ littermates, *Gnal*$^{+/-}$ mice exhibited increased catalepsy responses, persistent DNA breaks, decreased cAMP-dependent histone H3 phosphorylation (Ser10), and increased cell death in response to haloperidol. In striatum, aged *Gnal*$^{+/-}$ mice exhibited increased global DNA methylation, increased euchromatin, and dendritic structural abnormalities. Our results provide evidence that Gα(olf) deficiency intensifies the effects of D2R antagonism and suggests that loss-of-function variants in *GNAL* may increase risk for movement disorders associated with D2R blockers. We hypothesize that the effects of Gα(olf) dysfunction and/or long-term D2R antagonism may lead to epigenetic silencing, transcriptional dysregulation, and, ultimately, cellular senescence and/or apoptosis in human brain.

1. Introduction

GNAL encodes Gα(olf), the α subunit of a heterotrimeric GTP-binding protein (G-protein) which couples to downstream signaling partners including, but not limited to, adenylyl cyclase (Corvol et al., 2001; Herve et al., 1993). Initially identified in sensory neurons of the olfactory epithelium, Gα(olf) is highly enriched in the striatum, where it positively couples with dopamine D1 receptors (D1Rs) and adenosine A2A receptors (A2ARs) to activate adenylyl cyclase (Belluscio et al., 1998; Corvol et al., 2001), thereby increasing intracellular cAMP levels in D1R-expressing striatonigral (direct pathway MSNs, dMSNs) and D2R-expressing striatopallidal (indirect pathway MSNs, iMSNs) neurons, respectively. Gα(olf) levels serve as a determinant of cAMP signal-dependent activity in both dMSNs and iMSNs (Corvol et al., 2001; Herve et al., 2001; Morigaki et al., 2017).

Dystonia is a neurological movement disorder characterized by sustained or intermittent muscle contractions causing abnormal, often repetitive, movements, postures, or both (Albanese et al., 2013). Etiological categories include isolated dystonia and secondary dystonia. Autosomal dominant, loss-of-function mutations in *GNAL* have been associated with adult-onset isolated cervical and segmental dystonia (Fuchs et al., 2013; Vemula et al., 2013), and autosomal-recessive *GNAL* mutations are associated with early-onset generalized dystonia with mild intellectual disability (Masuho et al., 2016). *Gnal*$^{+/-}$ mice express approximately half of the normal levels of Gα(olf) without a compensatory increase in $G\alpha_s$ expression (Corvol et al., 2001; Herve

* Correspondence to: M. M. Khan, University of Tennessee Health Science Center, Department of Neurology, 434 Johnson Building, Memphis, TN 38163, USA.
** Correspondence to: M. S. LeDoux, University of Memphis, Department of Psychology, 400 Innovation Drive, Room 202, Memphis, TN 38152, USA.
E-mail addresses: mkhan26@uthsc.edu (M.M. Khan), msledoux@memphis.edu (M.S. LeDoux).

https://doi.org/10.1016/j.expneurol.2019.04.014
Received 23 September 2018; Received in revised form 9 April 2019; Accepted 23 April 2019
Available online 26 April 2019
0014-4886/

et al., 2001; Pelosi et al., 2017). Tardive dystonia is a persistent secondary dystonia that occurs after prolonged (> 6 months) treatment with antipsychotics and antiemetics that block D2Rs. D2R blockers can also cause acute transient dystonia. The cellular pathobiological relationships among acute and tardive dystonia caused by D2R blockers and isolated dystonia remain poorly understood. Haloperidol, a D2R blocker and widely prescribed antipsychotic, induces prolonged increases in histone H3 phosphorylation (Ser10) and chromatin remodeling in dopamine D2R-expressing neurons of the dorsomedial and dorsolateral striatum and this effect is mediated through activation of Gα(olf) (Bertran-Gonzalez et al., 2009; Li et al., 2004). Therefore, study of Gα(olf) provides a conduit for understanding the relationship between isolated and drug-induced dystonia.

Herein, we report that *Gnal*$^{+/-}$ mice showed sustained DNA breaks, decreased cAMP-dependent histone H3 phosphorylation (Ser10), abnormal motor behavior and increased cell death following haloperidol treatment. Aged *Gnal*$^{+/-}$ mice exhibited increased DNA methylation, increased euchromatin, and MSN dysmorphology. Overall, these findings suggest that Gα(olf) deficiency and, possibly, chronic D2R blockade, may lead to persistent alterations in chromatin structure and defective DNA repair which may contribute to epigenetic silencing, transcriptional dysregulation, and, ultimately, cellular senescence or death.

2. Materials and methods

2.1. Maintenance and breeding of mice

Gnal$^{+/-}$ mice and wild-type isogenic (*Gnal*$^{+/+}$) littermates were used in the experiments described here. *Gnal*$^{-/-}$ mice nurse poorly and typically die within 2 to 4 days after birth (Belluscio et al., 1998). Only rarely do *Gnal*$^{-/-}$ mice survive to adulthood (Belluscio et al., 1998). All mouse experiments were performed in accordance with the National Institutes of Health's Guidelines for the Care and Use of Laboratory Animals and approved by our Institutional Animal Care and Use Committee.

2.2. Biogenic monoamines

Abnormal striatal monoamine levels have reported in several mouse models of dystonia (Rose et al., 2015; Yokoi et al., 2006; Zhao et al., 2008) but, to our knowledge, have not yet been described in *Gnal*$^{+/-}$ mice. Therefore, to this end, striata were acutely harvested from 3 male and 3 female *Gnal*$^{+/+}$ and *Gnal*$^{+/-}$ mice at 10 months-of-age. All subsequent processing was completed by the Vanderbilt University Neurochemistry Core as previously described (Xiao et al., 2017). Briefly, tissue samples were homogenized with a dismembrator in a solution (pH 3.8) containing 100 mM trichloroacetic acid (TCA), 10 mM sodium acetate, 0.1 mM EDTA, 5 ng/ml isoproterenol (as internal standard) and 10.5% methanol. Homogenates (10 μl) were collected for assay of protein concentrations. Samples were then spun in a microcentrifuge at 10,000 ×*g* for 20 min and the supernatant was removed for monoamine analysis. Biogenic amines were determined by high-pressure liquid chromatography utilizing an Antec Decade II (oxidation: 0.65) electrochemical detector operated at 33 °C. Supernatants (20 μl) were injected using a Water 2707 autosampler onto a Phenomenex Kintex (2.6 u, 100 A) C18 HPLC column (100 × 4.60 mm). Biogenic amines were eluted with a mobile phase consisting of 89.5% 100 mM TCA, 10 mM sodium acetate, 0.1 mM EDTA and 10.5% methanol (pH 3.8). Solvents were delivered at 0.6 ml/min using a Waters 515 HPLC pump. Using this HPLC solvent biogenic amines were eluted in the following order: noradrenaline, 3, 4-dihydroxyphenylacetic acid (DOPAC); dopamine (DA); 5-hydroxyindoleacetic acid (5-HIAA); homovanillic acid (HVA); 5-hydroxytryptophan (5-HT); and 3-methoxytyramine (3-MT). HPLC control and data acquisition were managed by Empower software. Protein concentrations were determined with a BCA Protein Assay Kit (ThermoFisher Scientific, Waltham, MA, USA).

2.3. Haloperidol treatments

Mice of each genotype were randomized to treatment with either haloperidol (1 mg/kg intraperitoneal [IP]; Sigma-Aldrich, MO) or vehicle (saline containing 0.1% acetic acid) at 10 months-of-age. In pilot experiments, we performed dose-response effects (0.1, 0.5 and 1 mg/kg) of haloperidol to establish the optimal dose (Fig. S1). Additionally, the haloperidol dose (1 mg/kg body weight) chosen for our study provides optimal catalepsy responses in mice (Kim et al., 2008; Viyoch et al., 2001).

2.4. Behavioral assessments

Gnal$^{+/-}$ mice and sex-matched *Gnal*$^{+/+}$ littermates at 10 months-of-age were weighed (Fig. S2) and subjected to a battery of motor tests 3 and 6 h after haloperidol or vehicle treatments as previously described (Barnes et al., 1990; Khan et al., 2018; Xiao et al., 2017; Xiao et al., 2016). Motor testing was performed by investigators blinded to genotypes and treatment in the following order: raised beam task, rotarod, catalepsy, and open-field activity.

Mice were acclimated to an 80-cm long, 20-mm wide beam elevated 50 cm above a padded base. A 60 W lamp at the start served as an aversive stimulus, whereas the opposite end of the beam entered a darkened escape box. Slips were counted as mice traversed a 12-mm diameter square beam and traversal times were recorded. Single runs were performed at 3 and 6 h after injection of either haloperidol or vehicle.

Mice were acclimated to a Rotamex-5 rotarod (Columbus Instruments, Columbus, OH, USA) rotating at 5 rpm for 5 min on the day prior to data acquisition. On the following day, mice were exposed to a 30 s acclimation period at 4 rpm followed by an acceleration of 4 rpm every 30 s to a target of 40 rpm at 5 min. Rotarod activity was evaluated 3 and 6 h after haloperidol or vehicle injections.

Bar-test catalepsy was evaluated by placing both forepaws of the mouse over a horizontal bar (diameter: 1 cm), elevated 4 cm from floor (Barnes et al., 1990). The time during which the mouse maintained this position was recorded with a maximum duration of 180 s. The test was performed at 3 h and 6 h after haloperidol or vehicle treatment. The total amount of time that the mice remained in a cataleptic posture was calculated to give the cumulative catalepsy time for each group.

For assessment of open-field activity, mice were placed in commercially-available activity monitors (MED Associates) for 10-min sessions. The activity monitors measured 27 × 27 cm, with 16 infrared photocell beams equally spaced in the x and y axes of the horizontal plane, 1 cm from the chamber floor. An additional array of 16 photocells was situated 5 cm above the floor to track rearing. All tests were conducted in the dark. One hour prior to testing, cages were moved from the housing racks to a quiet anteroom adjacent to the testing room. Following this period of habituation, animals were removed from their home cage, immediately placed in the center of the open field and allowed to freely explore the apparatus for a test interval of 10 min. Animals were scored for a number of behaviors including total distance traveled (cm). The data recorded during testing was scored in post-session analyses using commercially-available software (Activity Monitor 5.1, Med Associates). Open-field activity was evaluated 3 h and 6 h after haloperidol or vehicle injections.

2.5. Immunohistochemistry

Fluorescent immunohistochemistry was performed as previously described (Khan et al., 2018). Briefly, mice were rapidly anesthetized with pentobarbital (100 mg/kg, IP) and transcardially perfused with 4% paraformaldehyde in 0.1 M sodium phosphate buffer (PB) (pH 7.4). Brains were removed and post-fixed in the same solution overnight and

cryo-protected with 30% sucrose in PB at 4 °C. Serial coronal sections of striatum of each group were cut on a cryostat (Leica) and incubated with blocking reagent (5% BSA and 1% goat serum in PBS) for 2 h at room temperature. Sections were then incubated overnight at 4 °C with one or more of the following primary antibodies: rabbit anti-53BP1 (#ab21083, Abcam), mouse anti-phospho-γ-H2A.X (Ser139) (#80312, Cell Signaling), mouse anti-D2R (#sc-5303, Santa Cruz) (Salti et al., 2015; Xiao et al., 2009), rabbit anti-phospho-histone H3 (Ser10) (#9701, Cell Signaling) and goat anti-ChAT antibody (#AB144P, Chemicon). TP53-binding protein 1 (53BP1) and phospho-γ-H2A.X (Ser139) serve as reliable markers of DNA double-strand breaks (DSBs). Terminal deoxynucleotidyl transferase dUTP nick-end labeling (TUNEL) staining was performed using a commercially available in situ Cell Death Detection kit (Roche Diagnostics). TUNEL staining, and 53BP1-, D2R-, and ChAT-immunohistochemistry was performed on brains harvested 6 h after injection of either haloperidol or vehicle. Immunohistochemistry for anti-phospho-γ-H2A.X (Ser139) and phospho-histone H3 (Ser10) was performed on brains harvested 1 h after injection of either haloperidol or vehicle. After washing in PBS, sections were incubated with their respective secondary antibodies (Invitrogen) for 1 h and washed 3× with PBS. Sections were cover-slipped in mounting media with DAPI or TO-PRO-3 (ThermoFisher Scientific). Images were captured with a Zeiss 710 laser scanning confocal microscope using a 40× oil objective with a numerical aperture of 1.3 and total magnification of 400×. TO-PRO-3 staining was used to identify MSNs and interneuron populations by their typical nuclear morphology (Matamales et al., 2009). Field of view (44,944 μm^2) was calculated using a scale bar overlay as reference. For quantification of 53BP1 colocalization with ChAT interneurons, D2R iMSNs, and TUNEL labeling, an investigator blinded to genotype and treatment examined 12 microscopic fields derived from 4 coronal sections per mouse brain (n = 3 mice/group).

Colocalization analysis of phospho-H2A.X (Ser139)- and phospho-histone H3 (Ser10)-immunohistochemistry was performed using Imaris (Bitplane) object-based colocalization software. Spot size was set at 0.5 μm and spot detection was based on mean intensity sums for each channel. Spots ≤0.5 μm from one another were considered colocalized. Colocalization was based on a total of 12 microscopic fields derived from 4 coronal sections per mouse brain (n = 3 mice/group).

2.6. Histone H3 phosporylation and cAMP ELISAs

The EpiQuik Global Histone H3 Phosphorylation (Ser10) ELISA (Epigentek, Farmingdale, NY) and cAMP ELISA (Cayman Chemical) kits were used to assess the phosphorylation of histone H3 (Ser10) and cAMP levels, respectively, at 10 months-of-age. In brief, mice were rapidly anesthetized with pentobarbital (100 mg/kg, IP) 1 h after injection of haloperidol or vehicle. Striata were dissected and homogenized in tissue extraction buffer for the quantification of histone H3 phosphorylation (Ser10) and cAMP levels. Results were expressed as % histone H3 phosphorylation (Ser10) compared to controls and pmols of cAMP/mg of protein, respectively.

2.7. Global DNA methylation

Quantification of global DNA methylation was performed using a commercially available MethylFlash Global DNA Methylation (5-mC) ELISA Easy Kit (Epigentek #P-1030). Genomic DNA was harvested from the striata of aged (18-month-old) *Gnal*$^{+/+}$ and *Gnal*$^{+/-}$ mice using the Classic™ Genomic DNA Isolation kit (Lamda Biotech, St. Louis, MO). For the quantification of 5-mC, 100 ng of DNA was added to a 96-well plate, followed by incubation with primary (anti-5-mC) and secondary antibodies and developed by colorimetric methods. The data was represented as percentage of 5-mC in total DNA.

2.8. Golgi staining

Brains of age-matched *Gnal*$^{+/-}$ and *Gnal*$^{+/+}$ littermates (n = 3/genotype, 18-months-old) were isolated and prepared according to standard Golgi–Cox impregnation technique using the FD Rapid GolgiStain™ Kit (FD NeuroTechnologies). Briefly, mice were rapidly anesthetized with pentobarbital and brains were quickly removed from the skull. After rinsing with water, brains were first immersed in the impregnation solution (A and B) which was replaced after 6 h and then kept in dark for 14 days with fresh impregnation solution. Afterwards, the brains were transferred to solution C overnight at room temperature. Serial cryostat sections of 100 μM were sagittally cut through both hemispheres of the mouse brain. Every first section of each series of 3 sections (interval: 300 μm) were mounted on gelatin-coated slides. Following staining in solutions D & E, sections were dehydrated in ethanol, cleared in xylenes and cover-slipped in Permount® (Fisher Scientific, Fair Lawn, NJ) for quantitative analysis. To assess dendritic morphology, low magnification images (*Z*-stack) of MSNs, were randomly selected using a bright field microscope. Images from *Gnal*$^{+/-}$ and *Gnal*$^{+/+}$ mice brains were manually traced using Neurolucida system (MicroBrightField). Total dendritic length and soma size were measured with NeurolucidaExplorer (MicroBrightField). Scholl analysis was performed to analyze number of intersections per shell starting from the point at the centroid of the cell body. The density of spines was quantified by counting the number of spines on the terminal segment of dendrites. Morphologic data from 8 neurons/mouse were averaged to provide a single data point for each animal.

2.9. Quantification of heterochromatin and euchromatin levels with transmission electron microscopy (TEM)

Gnal$^{+/-}$ mice and *Gnal*$^{+/+}$ littermates at 18 months-of-age were perfused with 4% paraformaldehyde/2% glutaraldehyde in 0.1 M sodium cacodylate buffer, pH 7.4. Whole brains were extracted and the dorsolateral striata were processed for TEM. Briefly, tissue was washed in 0.1 M sodium cacodylate and subsequently post-fixed in 1% osmium tetroxide, dehydrated with an ethanol series (50%, 70%, 90%, 95%, 100%), infiltrated using EmBed812 resin (Electron Microscopy Sciences), thin sectioned at 60 nm, and stained with UranyLess stain (Electron Microscopy Sciences). Grids were imaged on a JEOL-2000EX II TEM. Areas of heterochromatin were measured blindly using ImageJ threshold analysis and expressed as percent of nuclear area.

2.10. Statistical analysis

ANOVA with Sidak's post-hoc multiple comparisons test was used to determine the effects of genotype and treatment on parametric behavioral, biochemical and morphological measures. The Kruskal-Wallis test was used to compare treatment groups for a non-parametric behavioral measure (slips on the raised beam task) and Dunn's multiple comparisons test was used for pairwise post-hoc comparisons. Two-tailed *t*-tests were used to determine the effects of genotype on DNA methylation, TUNEL labeling, chromatin state, and biochemical measures. An alpha (α) of 0.05 was chosen for statistical significance.

3. Results

3.1. *Gnal*$^{+/-}$ mice have normal striatal monoamine levels

In contrast to DYT1, DYT11 and DYT5b mouse models of dystonia (Rose et al., 2015; Yokoi et al., 2006; Zhao et al., 2008), there was no effect of genotype on striatal monoamine levels (Table S1).

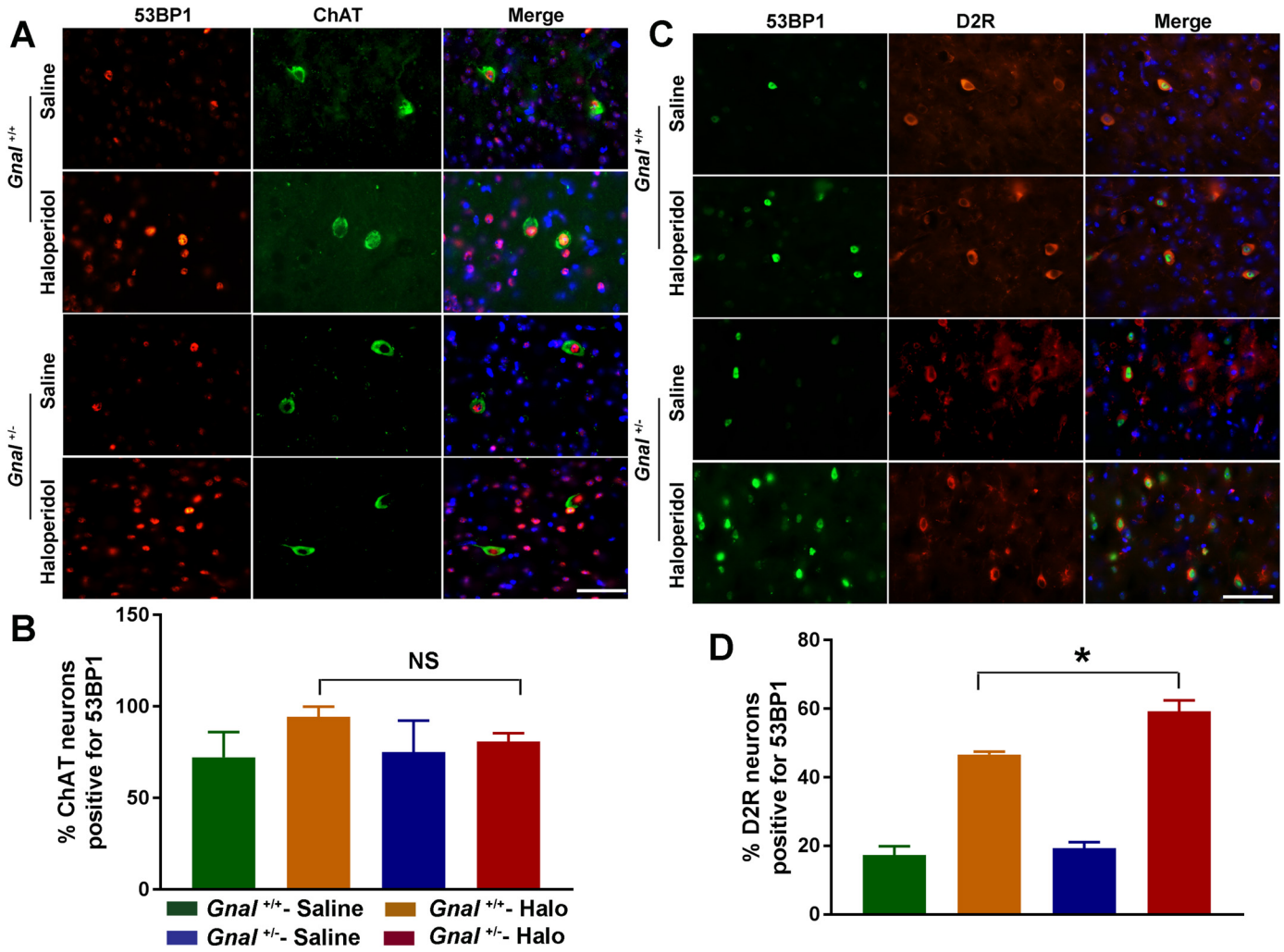

Fig. 1. *Gnal* haploinsufficiency is associated with increased numbers of persistent DSBs in the striatum of $Gnal^{+/-}$ mice. Representative images showing colocalization of 53BP1 with ChAT (A and B) and D2R (C and D) in $Gnal^{+/+}$ and $Gnal^{+/-}$ mice 6 h following haloperidol (1 mg/kg) or saline treatment. Scale bars = 50 μm.

3.2. Gnal haploinsufficiency is associated with persistent DNA damage and cell death in mouse brain following haloperidol treatment

Given the known effects of haloperidol on chromatin structure via histone H3 phosphorylation (Li et al., 2004) and report that haloperidol-treated fibroblasts show markedly depressed DNA transcription (Barak et al., 1996), we sought to determine if haloperidol treatment +/− Gα(olf) deficiency was associated with DNA damage in the striatum. We analyzed 53BP1-immunoreactivity in the striatum of $Gnal^{+/-}$ mice and $Gnal^{+/+}$ littermates mice treated with either haloperidol or vehicle. There were significant effects of treatment ($F_{1,8} = 45.45$, $p = .001$), genotype ($F_{1,8} = 9.36$, $p = .016$), and their interaction ($F_{1,8} = 7.15$, $p = .028$). After haloperidol treatment, we found that 53BP1-immunoreactive cells (Figs. 1 and 2) were more prevalent in the striatum of $Gnal^{+/-}$ mice when compared to their $Gnal^{+/+}$ littermates (adjusted $p = .022$). However, there were no significant differences in the basal levels of 53BP1-positive cells in the brains of vehicle treated $Gnal^{+/+}$ and $Gnal^{+/-}$ mice.

As seen in Fig. 1, striatal cholinergic interneurons were identified with ChAT-immunohistochemistry. D2R-immunohistochemistry, soma size and shape, and nuclear morphology were used to identify putative iMSNs. There was no effect of either treatment or genotype on the percentage of ChAT interneurons immunoreactive for 53BP1 (Fig. 1 a–b). Notably, however, a high percentage of ChAT interneurons were immunoreactive for 53BP1 in all experimental groups. In contrast, there was a clear increase in the percentage of 53BP1-immunoreactive D2R + neurons after treatment with haloperidol ($F_{1,8} = 234.6$, $p < .0001$; Fig. 1 c–d) and this effect was greater in $Gnal^{+/-}$ mice than $Gnal^{+/+}$ littermates ($p = .0085$). Although most of the 53BP1 + MSNs were putative iMSNs, there was also an increase in 53BP1 + putative dMSNs after haloperidol given that 53BP1 nuclear staining did not always co-localize with D2R immunoreactivity (Fig. 1c).

As shown in Fig. 2, TO-PRO-3 staining was used to localize DNA DSBs to either MSNs or striatal interneurons. There were significant effects of treatment ($F_{1,8} = 168.0$, $p < .0001$), genotype ($F_{1,8} = 17.3$, $p = .0033$), and the treatment*genotype interaction ($F_{1,8} = 13.93$, $p = .0058$) on the percentage of MSNs immunoreactive for 53BP1. There was a more robust effect of haloperidol in $Gnal^{+/-}$ mice in comparison with $Gnal^{+/+}$ littermates (adjusted $p = .0011$). Similarly, there were significant effects of treatment ($F_{1,8} = 113.9$, $p < .0001$), genotype ($F_{1,8} = 8.31$, $p = .021$), and the treatment*genotype interaction ($F_{1,8} = 7.90$, $p = .023$) on the percentage of TUNEL-positive MSNs. There was a larger effect of haloperidol in $Gnal^{+/-}$ mice in comparison with $Gnal^{+/+}$ littermates (adjusted $p = .0076$). In contrast, there were no significant effects of haloperidol or genotype on the numbers of 53BP1- or TUNEL-positive striatal interneurons. Taken together, these results suggest that Gα(olf) loss-of-function variants may increase risk for striatal DNA damage and cell death, particularly in iMSNs, in

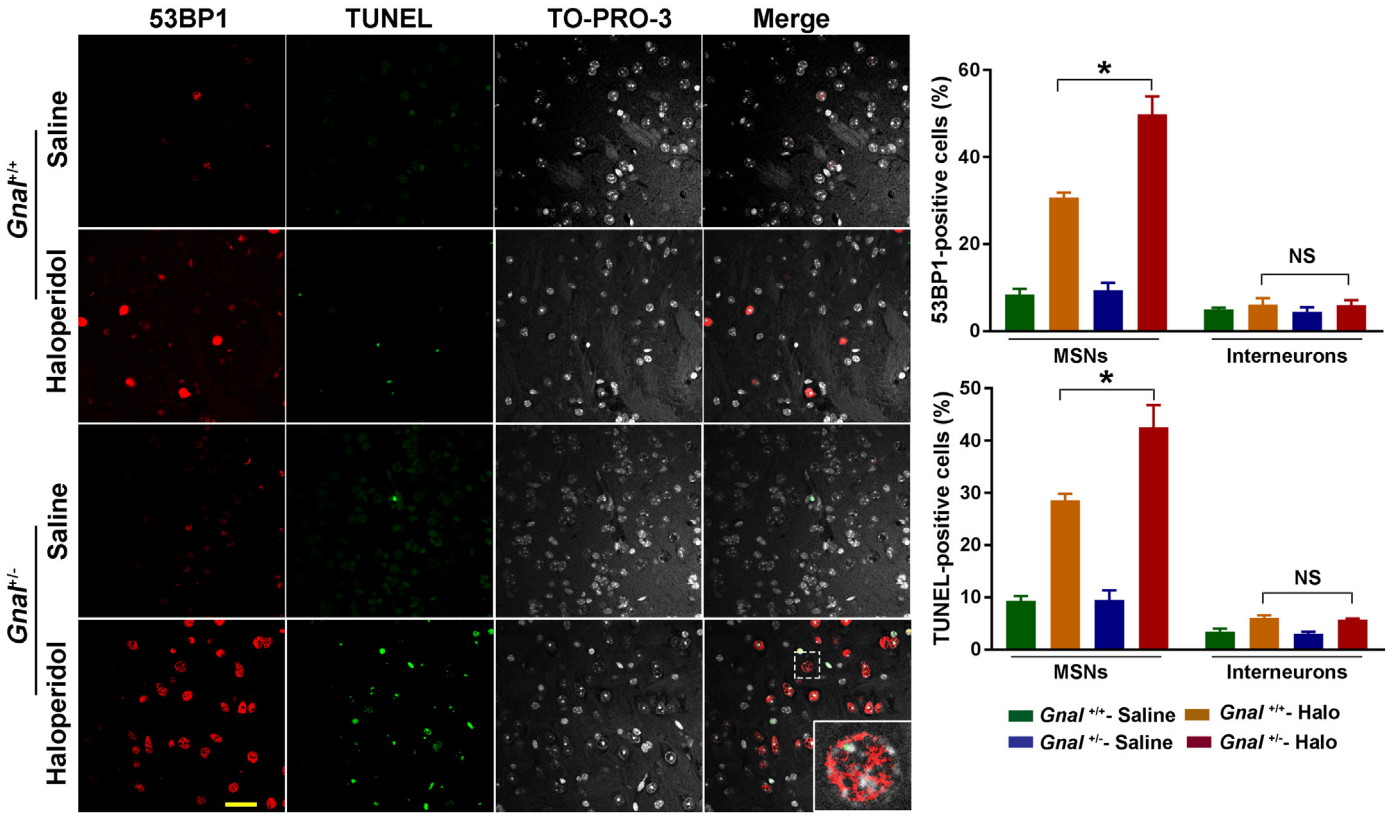

Fig. 2. *Gnal* haploinsufficiency was associated with increased apoptosis in the striatum following haloperidol (1 mg/kg) treatment. Brains were harvested from haloperidol- and saline-treated $Gnal^{+/-}$ mice and $Gnal^{+/+}$ littermates 6 h after treatment with haloperidol or saline and processed for TUNEL labeling, 53BP1 immunohistochemistry, and TO-PRO-3. TO-PRO-3 nuclear staining was used to classify cells as MSNs or non-MSNs (interneurons) and determine the percentage of cells that were positive for 53BP1 or TUNEL. Values are expressed as means ± SEM. Scale bar = 25 μm.

response to haloperidol and other D2-receptor blockers in human populations.

3.3. $Gnal^{+/-}$ mice show relatively reduced levels of cAMP and histone H3 phosphorylation following haloperidol treatment

Administration of the D2R-blocker haloperidol has been shown to promote cAMP-dependent signaling in striatal MSNs (Sibley and Monsma, 1992; Li et al., 2004; Pan et al., 2015). Gα(olf) is enriched in striatum where it positively couples with dopamine D1R and A2AR to increase intracellular cAMP levels (Corvol et al., 2001). We found significant effects of genotype ($Gnal^{+/+}$ vs. $Gnal^{+/-}$, $F_{1,28} = 7.82$, $p = .0092$) and treatment (saline vs. haloperidol, $F_{1,28} = 4.60$, $p = .041$) on cAMP levels but no genotype*treatment interaction. One hour following haloperidol treatment, $Gnal^{+/-}$ mice showed significantly decreased levels of cAMP as compared to $Gnal^{+/+}$ littermates (adjusted $p = .022$), suggesting that Gα(olf) levels may serve as one determinant of cAMP signal-dependent activity in striatum (Fig. S3A).

Histone H3 phosphorylation is a reversible dynamic process closely intertwined with long-term changes in chromatin structure that regulates both condensation of chromosomes with transcriptional repression and signal-induced gene activation (Sawicka and Seiser, 2012). Therefore, we sought to determine the synergistic effects of D2R blockade and Gα(olf) deficiency on histone H3 phosphorylation in mice 1 h after administration of haloperidol. Based on ELISA, there were significant effects of treatment ($F_{1,21} = 23.99$, $p < .001$) and genotype ($F_{1,21} = 13.26$, $p = .0015$) on histone H3 phosphorylation in striatum, but no treatment*genotype interaction ($F_{1,21} = 3.04$, $P = .096$). Post-hoc analyses showed that there was significantly less striatal histone H3 phosphorylation in $Gnal^{+/-}$ mice in comparison with their $Gnal^{+/+}$ littermates after treatment with haloperidol (Fig. S3B, adjusted $p = .0009$).

There was a significant effect of haloperidol ($F_{1,8} = 29.01$, $p = .0007$) but no effect of genotype ($F_{1,8} = 2.15$, $p = .18$) or the treatment*genotype interaction on phosphorylated γ-H2A.X (Ser139) labeling (Fig. S4). Similarly, there was a significant effect of haloperidol ($F_{1,8} = 19.34$, $p = .0023$) but no effect of genotype ($F_{1,8} = 3.80$, $p = .087$) or the treatment*genotype interaction on phosphorylated histone H3 (Ser10) labeling (Fig. S4). There was also a significant effect of haloperidol ($F_{1,8} = 14.23$, $p = .0054$) but no effect of genotype ($F_{1,8} = 0.40$, $p = .54$) or the treatment*genotype interaction on colocalization of phosphorylated γ-H2A.X (Ser139) and phosphorylated histone H3 (Ser10) labeling (Fig. S4). Colocalization of phosphorylated γ-H2A.X (Ser139) and phosphorylated histone H3 (Ser10) labeling increased after administration of haloperidol in both $Gnal^{+/+}$ and $Gnal^{+/-}$ mice.

3.4. *Gnal* haploinsufficiency is associated with enhanced behavioral abnormalities in response to haloperidol

$Gnal^{+/-}$ mice and $Gnal^{+/+}$ littermates were subjected to behavioral tests 3 and 6 h after the systemic administration of haloperidol or vehicle. Overall, there were no significant effects of time (3 h vs. 6 h) or sex (male vs. female). Two-way ANOVA was then used to independently examine the effects of haloperidol and genotype at each time point. Overall, we did not identify significance differences in motor functioning and cataleptic responses between vehicle-treated $Gnal^{+/+}$ and $Gnal^{+/-}$ mice. After treatment with haloperidol mice performed poorly on open-field activity (Table S2 and Fig. S5), a raised beam task (Fig. 3 a–b), and an accelerating rotarod (Fig. 3c). On open-field activity, there were no effects of genotype but significant effects of haloperidol on distances traveled, ambulatory counts, stereotypic

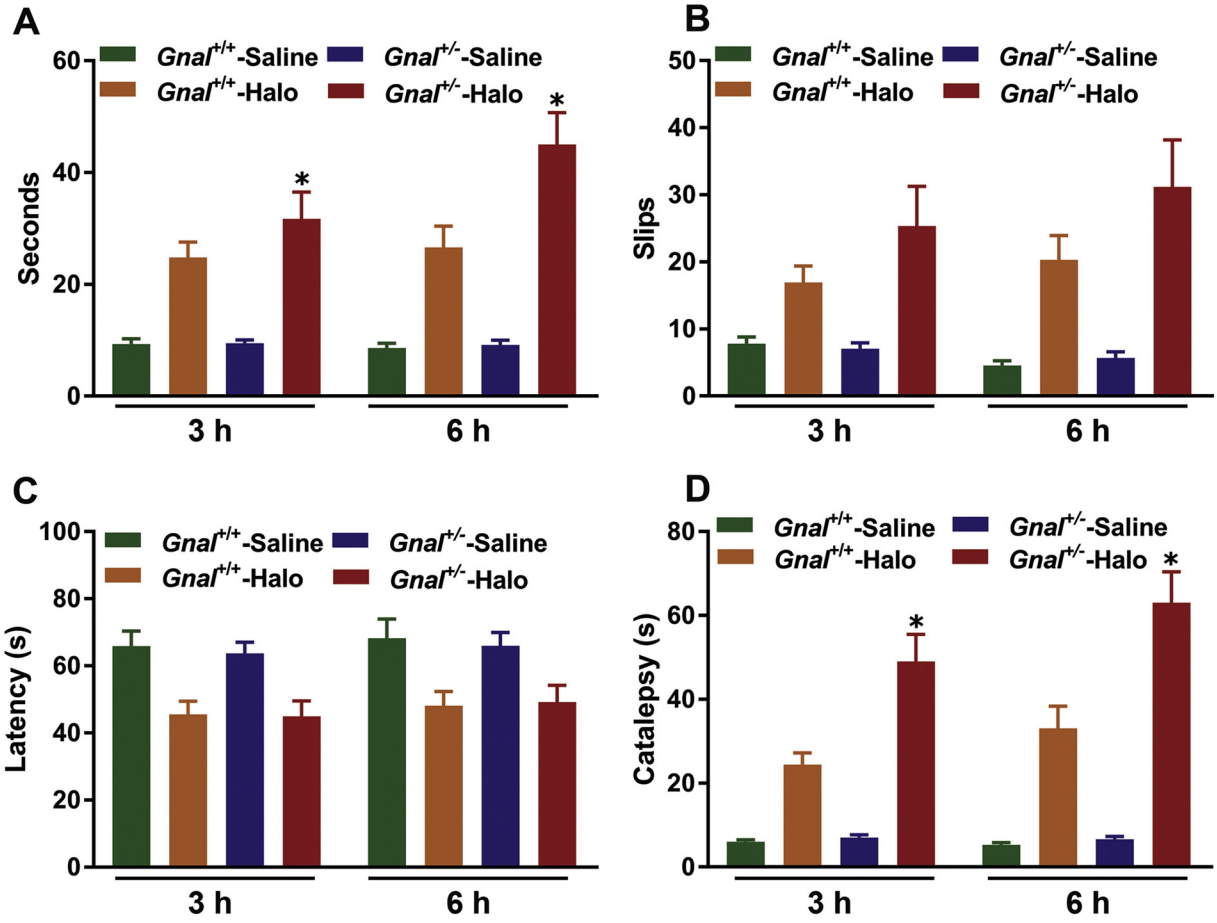

Fig. 3. Adult (10-month-old) *Gnal*$^{+/-}$ mice and sex-matched *Gnal*$^{+/+}$ littermates were analyzed with a battery of behavioral tests following haloperidol (1 mg/kg) or saline treatment (n = 16–18/group). A. Traversal time on raised beam task. B. Slips on raised beam task. C. Latency to fall from an accelerating rotarod. D. Catalepsy response to haloperidol. Values are expressed as means ± SEM. *significant effect of genotype ($p < .05$).

counts, and ambulatory episodes at both 3 and 6 h.

For traversal times on the raised beam task at 3 h, there was an overall effect of treatment ($F_{1,65} = 44.87$, $p < .0001$) and genotype ($F_{1,65} = 5.45$, $p = .023$) and a significant treatment*genotype interaction ($F_{1,65} = 5.34$, $p = .024$). Haloperidol had a larger effect in *Gnal*$^{+/-}$ than *Gnal*$^{+/+}$ mice (adjusted $p = .003$). Similarly, at 6 h there was an overall effect of treatment ($F_{1,65} = 83.9$, $p < .0001$) and genotype ($F_{1,65} = 11.68$, $p = .0011$) and a significant treatment*genotype interaction ($F_{1,65} = 11.16$, $p = .0014$). Haloperidol had a larger effect on *Gnal*$^{+/-}$ than *Gnal*$^{+/+}$ mice (adjusted $p < .0001$). In comparison to vehicle, there were significant effects of haloperidol on slips at 3 and 6 h ($p < .01$, for both), but no effect of genotype. There were significant effects of treatment at 3 h ($F_{1,65} = 22.71$, $p < .0001$) and 6 h ($F_{1,65} = 15.07$, $p = .0002$) but no effect of genotype on latencies to fall from an accelerating rotarod.

Prolonged catalepsy is a well-established effect of drugs that block D2Rs. In our study, there were robust effects of treatment and genotype on catalepsy (Fig. 3d). At 3 h, there were significant effects of treatment ($F_{1,71} = 71.37$, $p < .0001$), genotype ($F_{1,71} = 12.99$, $p = .0006$), and the treatment*genotype interaction ($F_{1,71} = 10.84$, $p = .0015$). In comparison to *Gnal*$^{+/+}$ littermates, there was a larger effect of haloperidol on *Gnal*$^{+/-}$ mice (adjusted $p < .0001$). Similarly, at 6 h, there were significant effects of treatment ($F_{1,71} = 85.00$, $p < .0001$), genotype ($F_{1,71} = 12.75$, $p = .0006$), and the treatment*genotype interaction ($F_{1,71} = 11.01$, $p = .0014$). In comparison to *Gnal*$^{+/+}$ littermates, there was a larger effect of haloperidol on *Gnal*$^{+/-}$ mice (adjusted $p < .0001$).

3.5. *Gnal haploinsufficiency is associated with increased global DNA methylation in aged mouse brain*

DNA methylation is an essential epigenetic mechanism that regulates gene expression and the maintenance of DNA integrity and stability (Razin and Kantor, 2005; Schar and Fritsch, 2011). Therefore, epigenetic modifications likely play an important role in several neurological disorders. In our study, we found that aged *Gnal*$^{+/-}$ mice showed increased global DNA methylation in striatum (Fig. S6) suggesting the possibilities of epigenetic silencing, transcriptional dysregulation, and, possibly, eventual chromatin condensation and cellular senescence.

3.6. *Morphological changes in medium spiny neurons of Gnal*$^{+/-}$ *mice as assessed by Golgi staining*

Golgi analyses (Fig. 4) showed no significant effects of genotype on total dendritic length (Fig. 4b) or soma size (Fig. 4c). However, in-depth morphometric analysis with the Sholl method, where dendrites arising from the soma were examined within concentric three-dimensional shells of increasing diameter (10 μm) centered around the cell body, showed that, at distances of 30 to 60 μm from the soma, *Gnal*$^{+/-}$ MSN dendrites were less elaborate than those from littermate controls (Fig. 4d), and there were fewer cumulative Sholl hits in *Gnal*$^{+/-}$ MSNs (Fig. 4e). However, there were no differences in dendritic spine numbers on terminal branch segments of the two experimental groups (Fig. 4 f–g).

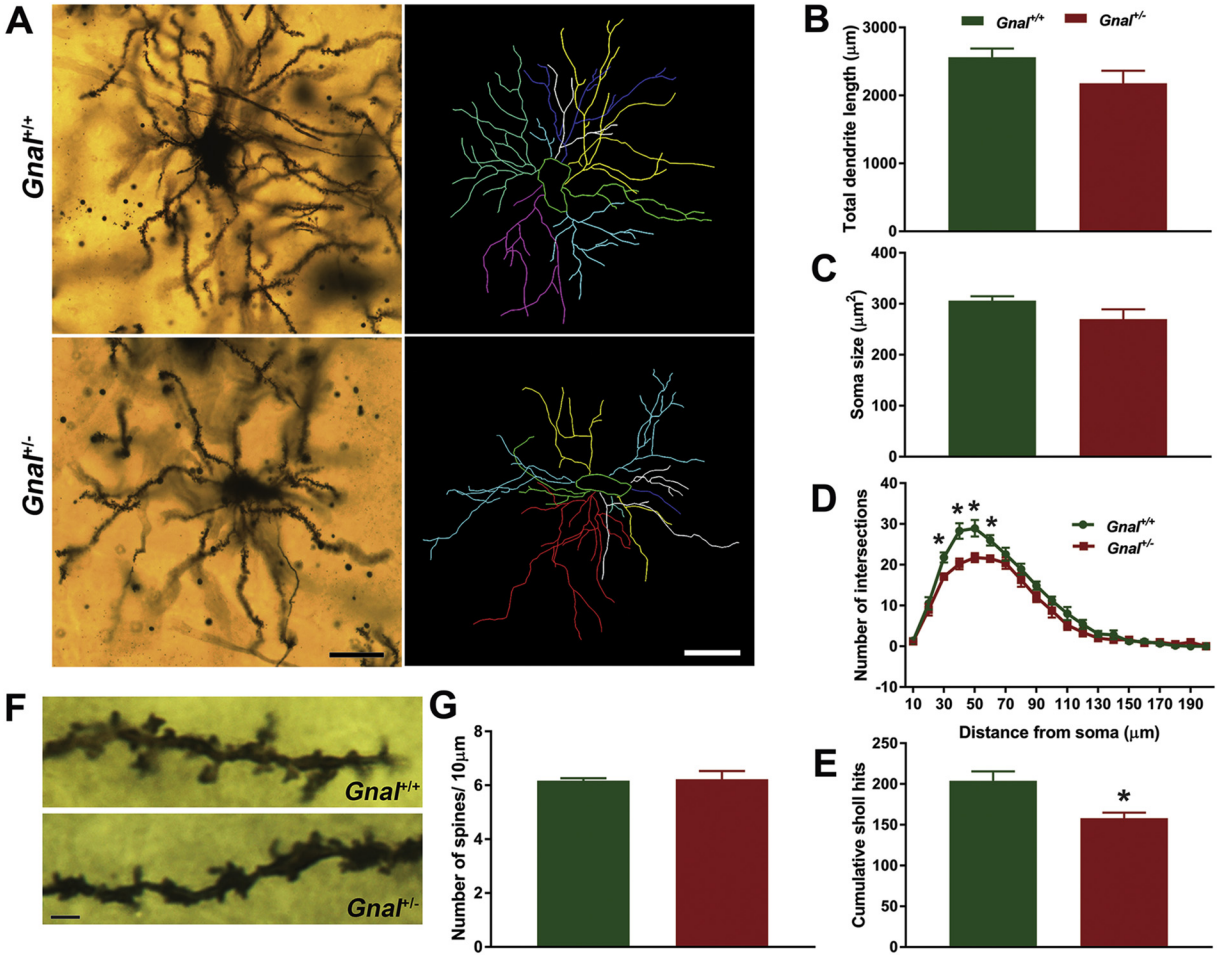

Fig. 4. Morphometry of striatal MSNs from 18-month-old mice. A. Representative microphotographs of *Gnal*$^{+/+}$ and *Gnal*$^{+/-}$ Golgi-stained MSNs and their 3D reconstruction with Neurolucida software. Quantitative analysis of total dendrite length (B) and soma size (C). Sholl analysis showed reduction in dendritic branching in the inner two thirds of the dendritic arbor (D) and decreased cumulative Sholl hits (E) in the inner portion of the dendritic arbor of *Gnal*$^{+/-}$ MSNs (1–140 μm). F and G. There was no effect of genotype on dendritic spine density. Scale bar = 10 μm. Values are expressed as means ± SEM (n = 3/genotype). *p < .05.

3.7. *Gnal* haploinsufficiency alters chromatin accessibility

Chromatin protects template DNA and modifications of chromatin structure exert important effects on gene expression, genome stability and cell survival. A more relaxed chromatin conformation is prone to both exogenous and endogenous damage often leading to enhanced activation of the DNA damage response. Accordingly, we quantified the ratio of heterochromatin to euchromatin with TEM. TEM analyses showed that there was a more relaxed and open chromatin conformation in aged *Gnal*$^{+/-}$ mice as compared to *Gnal*$^{+/+}$ littermates as measured by the heterochromatin/euchromatin ratio (Fig. 5).

4. Discussion

Haloperidol treatment was associated with reduced striatal cAMP and histone H3 phosphorylation, and increased DNA damage, apoptotic cell death, and catalepsy in *Gnal*$^{+/-}$ mice. These effects were not due to overt defects in dopamine synthesis or turnover. Although increased catalepsy is seemingly paradoxical in the context of reduced haloperidol-induced cAMP, the various neuronal and pharmacological substrates that drive catalepsy have not been clearly harmonized (Sanberg et al., 1988; Barnes et al., 1990; Wadenberg et al., 1996; Viyoch et al., 2001).

Aged *Gnal*$^{+/-}$ mice showed abnormal MSN dendritic structure, increased euchromatin in the dorsolateral striatum, and increased striatal global DNA methylation. These findings suggest that Gα(olf) deficiency could contribute to persistent increases in open chromatin independent of effects on histone H3 phosphorylation, which is but one of many contributors to chromatin structure. This relative euchromatin state could, in turn, contribute to the accumulation of DNA damage and epigenetic silencing of unrepaired DNA with resultant alterations in gene expression and neuronal morphology. However, the relative short lifespan of mice, in comparison with humans, may not permit ultimate conversion to a heterochromatin state.

Gnal encodes Gα(olf) and XLGα(olf) which are both expressed in human striatum (Vemula et al., 2013). Gα(olf) refers to the major isoform (381 aa) and XLGα(olf) to the long isoform (458 aa). XLGα(olf) has shown Golgi and perinuclear expression in transfected Cos7 cells (Akita et al., 2009) and antibodies targeting both XLGα(olf)/Gα(olf) have shown evidence for both nuclear and cytoplasmic localization (The Human Protein Atlas, www.proteinatlas.org) (Vemula et al., 2013). Using cNLS Mapper (Kosugi et al., 2009), NLStradamas (Nguyen Ba et al., 2009), and NucPred (Brameier et al., 2007) both human (NP_892023.1, 458 aa) and mouse (NP_796111.2, 448 aa) XLGα(olf) are found to harbor predicted nuclear localization signals. Mouse and human XLGα(olf) show 91% identities and 92% positives (BLAST, blast.ncbi.nlm.nih.gov/) although conservation is weakest in the N-terminal quarters of these two proteins. XLGα(olf)/Gα(olf) has been shown to interact with USP3 (ubiquitin specific peptidase 3), BABAM1 (alias - MERIT40, BRISC and BRCA1 A complex member 1), and SPATA2 (spermatogenesis associated 2) (Jensen et al., 2009; Kerrien et al., 2007; Stark et al., 2011). Furthermore, XLGα(olf) regulates expression

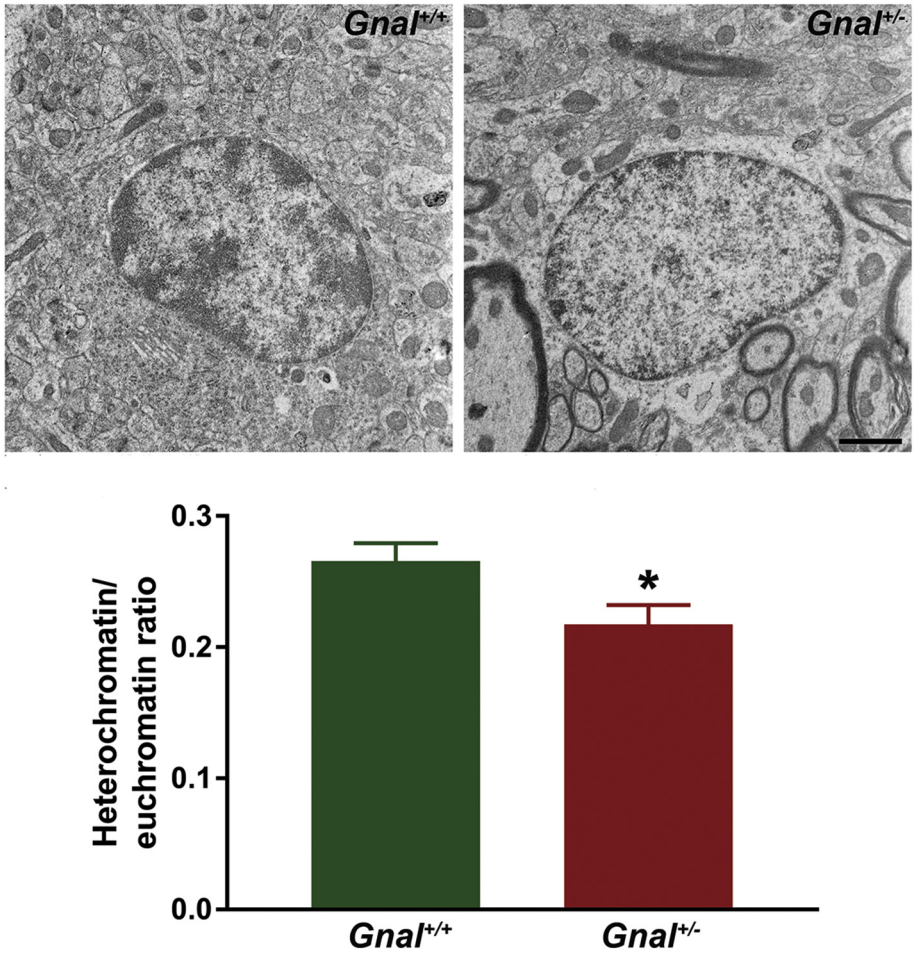

Fig. 5. Striatal TEM images from 18-month-old *Gnal*$^{+/-}$ mice and *Gnal*$^{+/+}$ littermates showing heterochromatin and euchromatin organization and their quantification. Values are expressed as means ± SEM. (n = 3 mice/genotype, *p = .018).

of CDKN1B (cyclin-dependent kinase inhibitor 1B [p27^{Kip1}]) in a COPS5 (COP9 signalosome subunit 5 variant) and CKD2 dependent manner (Akita et al., 2011). Several of these interactions point to a direct role for XLGα(olf) in DNA damage repair and cell-cycle control, independent of Gα(olf)'s role in histone H3 phosphorylation. CDKN1B is involved in control of cell cycle progression at G1/S (Akita et al., 2011). MERIT40 acts early in the DNA damage response and regulates localization of BRCA1 to DNA DSBs (Feng et al., 2009). SPATA2 is an essential component of the tumor necrosis factor α-receptor signaling complex (TNF-RSC). Downregulation of SPATA2 augments transcriptional activation of NF-κB and inhibits TNFα-induced necroptosis (Wagner et al., 2016). In this regard, NF-κB was a major hub for upregulated genes in the *Ciz1* KO model of dystonia (Xiao et al., 2016). Therefore, it is conceivable that loss of Gα(olf)/XLGα(olf) function could disturb homeostatic mechanisms involved in DNA repair and maintenance of chromatin structure ultimately leading to accumulation of unrepaired, erroneously repaired, and epigenetically-silenced DNA with consequent transcriptional dysregulation.

Gene expression studies were previously used to identify pathways possibly dysregulated by mutant Gα(olf)/XLGα(olf) in humans (Vemula et al., 2013). The top dysregulated networks in lymphoblastoid cell lines were involved in cell-cycle control, development, cell death and cellular proliferation (Vemula et al., 2013). Mutations in other genes (*THAP1*, *CIZ1*, *KMT2B*, *TAF1*, *ATM*) that encode proteins involved in cell-cycle and DNA repair have been linked to dystonia (LeDoux et al., 2013; Meyer et al., 2017). Although the consequences of defective DNA damage repair have been well-characterized in proliferating cells, the precise roles of these pathways and associated proteins remain poorly understood in post-mitotic neurons. In MSNs, dopamine D1Rs and A2ARs are coupled to adenylyl-cyclase through a heterotrimeric G-protein composed of Gα(olf), Gβ2, and Gγ7 subunits (Beaulieu et al., 2015; Corvol et al., 2004; Corvol et al., 2001). Histone H3 phosphorylation is under the opposite tonic control of D2Rs and A2ARs (Bertran-Gonzalez et al., 2009). Histone H3 phosphorylation at Ser10 inhibits checkpoint kinase 1, a key component of the ATM/ATR arm of the G1/S checkpoint pathway (Liokatis et al., 2012). In post-mitotic neurons, much of this checkpoint pathway (e.g., ATM) participates in the repair of DNA DSBs and other lesions of DNA including single-strand breaks, stalled replication, and mismatches. Moreover, DNA repair is intimately linked to chromatin structure through histone modifications including acetylation and methylation of histone H3 (House et al., 2014).

The altered chromatin organization seen in aged Gα(olf)-deficient mice could be driven by a variety of mechanisms independent of H3 phosphorylation given that no significant differences were noted in H3 phosphorylation between *Gnal*$^{+/+}$ and *Gnal*$^{+/-}$ mice at baseline. In particular, DNA damage can cause heterochromatin unfolding and altered chromatin accessibility (Nair et al., 2017). In theory, persistent modifications to chromatin structure or other epigenetic changes could contribute to the development of tardive dystonia after prolonged exposure to D2R blockers or isolated dystonia after decades of Gα(olf) deficiency (Li et al., 2004; Nicholas et al., 2008). Moreover, it is reasonable to assume that the acute effects of D2R blockers on H3 phosphorylation and other chromatin modifications show important differences from chronic effects.

In MSNs, haloperidol-induced activation of cAMP-dependent protein kinase A (PKA) and of the protein phosphatase-1 inhibitor,

dopamine- and cAMP-regulated phosphoprotein of 32 kDa (DARPP-32), has been proposed to affect gene transcription by acting on nuclear targets, including the cAMP response element-binding protein and histone H3 (Bertran-Gonzalez et al., 2009; Pozzi et al., 2003; Valjent et al., 2011). Consistent with previously published data showing that treatment with D2-like antagonists rapidly induces the phosphorylation of histone H3 at Ser 10 in bulk striatal chromatin (Li et al., 2004), we found that Gα(olf) deficiency attenuated the effects of haloperidol on cAMP levels and H3 phosphorylation. On the other hand, there was no significant effect of genotype on basal levels of cAMP. Similarly, in Huntington disease models, phosphodiesterase 10 (PDE10) loss was not accompanied by significant alternations in basal levels of striatal cAMP suggesting that loss of PDE10 could be balanced by alterations in cyclic nucleotide generation (Beaumont et al., 2016). Moreover, cAMP is also present in astrocytes and other striatal cell types that do not express important amounts of Gα(olf) (Uhernik et al., 2014; Zhou et al., 2019).

Although we observed that aged *Gnal*$^{+/-}$ mice displayed increased global DNA methylation in the striatum, we did not establish a clear link to H3 phosphorylation or the DNA damage response. First of all, histone H3 phosphorylation is a reversible dynamic process closely intertwined with long-term changes in DNA that regulates both (1) condensation of chromosomes with transcriptional repression and (2) signal-induced gene activation (Sawicka and Seiser, 2012). Second, D1- and D2-receptor signaling can induce changes in chromatin and transcription via ERK1/2, TOR, and cAMP/PKA signaling cascades. These cascades do not operate in isolation and exhibit a moderate degree of cross-talk and redundancy. For example, mitogen and stress-activated kinase-1, a nuclear target of ERK1/2, phosphorylates histone H3. Third, we only examined one of a multitude of histone post-translational modifications. Finally, a growing body of evidence suggests that histone modifications can contribute to DNA methylation through an assortment of direct and indirect mechanisms (Cedar and Bergman, 2009; LeDoux et al., 2016).

Golgi analysis showed that 18-month-old *Gnal*$^{+/-}$ mice had reductions in dendritic branching and decreased cumulative Sholl hits in the inner dendritic arbor of MSNs. However, we did not determine if these findings were specific to dMSNs or iMSNs, or exclusive to the striatum. We also found increased cell death in *Gnal*$^{+/-}$ mice following systemic administration of haloperidol. In previous work using a different methodology, slight reductions in MSN spine lengths were seen in the dorsolateral striata of 12-month-old *Gnal*$^{+/-}$ mice (Pelosi et al., 2017). Because younger mice were not assessed in these two studies, we cannot exclude the possibility that Gα(olf) deficiency exerts a developmental effect on neuronal morphology. On the other hand, given that human *GNAL*-associated dystonia develops after decades of Gα(olf) deficiency, these pathological changes in the mouse striatum may be more severe in humans with dystonia-associated GNAL mutations.

Gnal$^{+/-}$ mice did not exhibit dystonia or dyskinesias but they did show increased sensitivity to the negative motor effects of haloperidol despite relatively low striatal cAMP. Although genetic deletion of DARPP-32 in iMSNs was reported to increase locomotor activity and reduce cataleptic responses to haloperidol (Bateup et al., 2010), catalepsy was also reduced in mice with selective deletion of D2Rs on striatal cholinergic interneurons (Dawson et al., 1988; McVittie et al., 1991; Kharkwal et al., 2016), and D3R blockade in the cerebellum reduces the cataleptic effects of haloperidol (Shimizu et al., 2014). In addition to MSNs and cerebellar Purkinje cells, Gα(olf) is also expressed in the cerebellar nuclei and cerebral cortex. In the striatum, cholinergic interneurons express both Gα(olf) and Gαs and the consequences Gα(olf) deficiency on Gαs expression in this neuronal population has not been reported. Interpretation of our behavioral results is further complicated by the fact that both serotonin and dopamine have been implicated in the neuropharmacology of catalepsy and haloperidol acts on numerous receptors including D2, D3, D4, σ1, and 5HT2A (Wadenberg, 1996; Wadenberg et al., 1996). Finally, technical aspects of catalepsy protocols including drug dosages can lead to confounds when comparing data among studies (Sanberg et al., 1988).

In previously-published work, rare surviving homozygous null mice (*Gnal*$^{-/-}$) were noted to manifest hyperactive behavior (Belluscio et al., 1998) and systemic administration of a cholinergic agonist, oxotremorine, was associated with abnormal motor postures (Pelosi et al., 2017). This latter finding suggests that striatal cholinergic interneurons may also be involved in the pathobiology of *GNAL*-associated dystonia in humans. Conditional models will be required to define the relative contributions of specific cell types and receptors in the pathophysiology of positive and negative motor signs associated with Gα(olf) deficiency.

Our findings suggest that the motor side effects produced by D2R antagonism and Gα(olf) deficiency may be linked to DNA damage and/or epigenetic changes with resultant alterations in chromatic structure (Swathy and Banerjee, 2017). This, in turn, could lead to the accumulation of DNA breaks and epigenetic silencing with resultant aberrant transcription leading to neuronal dysmorphology and, ultimately, cellular senescence or death (Barak et al., 1996). Future studies using chronic D2R blockade in *Gnal*$^{+/-}$ mice will be required to establish more robust links between chromatin structure, accumulation of DNA damage, epigenetic changes and gene expression.

Disclosure statement

The authors declare no potential conflicts of interest.

Acknowledgements

This study was supported by the Dorothy/Daniel Gerwin Parkinson's Research Fund; Department of Defense grant W81XWH-17-1-0062; National Institutes of Health (NIH) grants R01 NS082296, R01 NS069936, R21 GM118962, R03 NS101485, R56 NS094965, and P30 DA033934; the University of Tennessee Health Science Center Neuroscience Institute; and the Division of Rehabilitation Sciences, College of Health Professions, University of Tennessee Health Science Center.

Appendix A. Supplementary data

Supplementary data to this article can be found online at https://doi.org/10.1016/j.expneurol.2019.04.014.

References

Akita, K., Takahashi, Y., Kataoka, M., Saito, K., Kaneko, H., 2009. Subcellular localization of a novel G protein XLGalpha(olf). Biochem. Biophys. Res. Commun. 381, 582–586.
Akita, K., Takahashi, Y., Takata, N., Hashimoto, M., Kataoka, M., Tomigahara, Y., Saito, K., 2011. XLGalphaolf regulates expression of p27Kip1 in a CSN5 and CDK2 dependent manner. Biochem. Biophys. Res. Commun. 416, 385–390.
Albanese, A., Bhatia, K., Bressman, S.B., Delong, M.R., Fahn, S., Fung, V.S., Hallett, M., Jankovic, J., Jinnah, H.A., Klein, C., Lang, A.E., Mink, J.W., Teller, J.K., 2013. Phenomenology and classification of dystonia: a consensus update. Mov. Disord. 28, 863–873.
Barak, Y., Ron, I.G., Sirota, P., Sobe, T., Slor, H., 1996. The effect of chlorpromazine and haloperidol on DNA transcription. Int. Clin. Psychopharmacol. 11, 193–197.
Barnes, D.E., Robinson, B., Csernansky, J.G., Bellows, E.P., 1990. Sensitization versus tolerance to haloperidol-induced catalepsy: multiple determinants. Pharmacol. Biochem. Behav. 36, 883–887.
Bateup, H.S., Santini, E., Shen, W., Birnbaum, S., Valjent, E., Surmeier, D.J., Fisone, G., Nestler, E.J., Greengard, P., 2010. Distinct subclasses of medium spiny neurons differentially regulate striatal motor behaviors. Proc. Natl. Acad. Sci. U. S. A. 107, 14845–14850.
Beaulieu, J.M., Espinoza, S., Gainetdinov, R.R., 2015. Dopamine receptors - IUPHAR review 13. Br. J. Pharmacol. 172, 1–23.
Beaumont, V., Zhong, S., Lin, H., Xu, W., Bradaia, A., Steidl, E., Gleyzes, M., Wadel, K., Buisson, B., Padovan-Neto, F.E., et al., 2016. Phosphodiesterase 10A inhibition improves cortico-basal ganglia function in Huntington's disease models. Neuron 92, 1220–1237.
Belluscio, L., Gold, G.H., Nemes, A., Axel, R., 1998. Mice deficient in G(olf) are anosmic. Neuron 20, 69–81.
Bertran-Gonzalez, J., Hakansson, K., Borgkvist, A., Irinopoulou, T., Brami-Cherrier, K., Usiello, A., Greengard, P., Herve, D., Girault, J.A., Valjent, E., Fisone, G., 2009. Histone H3 phosphorylation is under the opposite tonic control of dopamine D2 and

adenosine A2A receptors in striatopallidal neurons. Neuropsychopharmacology 34, 1710–1720.
Brameier, M., Krings, A., MacCallum, R.M., 2007. NucPred—predicting nuclear localization of proteins. Bioinformatics 23, 1159–1160.
Cedar, H., Bergman, Y., 2009. Linking DNA methylation and histone modification: patterns and paradigms. Nat. Rev. Genet. 10, 295–304.
Corvol, J.C., Studler, J.M., Schonn, J.S., Girault, J.A., Herve, D., 2001. Galpha(olf) is necessary for coupling D1 and A2a receptors to adenylyl cyclase in the striatum. J. Neurochem. 76, 1585–1588.
Corvol, J.C., Muriel, M.P., Valjent, E., Feger, J., Hanoun, N., Girault, J.A., Hirsch, E.C., Herve, D., 2004. Persistent increase in olfactory type G-protein alpha subunit levels may underlie D1 receptor functional hypersensitivity in Parkinson disease. J. Neurosci. 24, 7007–7014.
Dawson, V.L., Dawson, T.M., Filloux, F.M., Wamsley, J.K., 1988. Evidence for dopamine D-2 receptors on cholinergic interneurons in the rat caudate-putamen. Life Sci. 42, 1933–1939.
Feng, L., Huang, J., Chen, J., 2009. MERIT40 facilitates BRCA1 localization and DNA damage repair. Genes Dev. 23, 719–728.
Fuchs, T., Saunders-Pullman, R., Masuho, I., Luciano, M.S., Raymond, D., Factor, S., Lang, A.E., Liang, T.W., Trosch, R.M., White, S., et al., 2013. Mutations in GNAL cause primary torsion dystonia. Nat. Genet. 45, 88–92.
Herve, D., Levi-Strauss, M., Marey-Semper, I., Verney, C., Tassin, J.P., Glowinski, J., Girault, J.A., 1993. G(olf) and Gs in rat basal ganglia: possible involvement of G(olf) in the coupling of dopamine D1 receptor with adenylyl cyclase. J. Neurosci. 13, 2237–2248.
Herve, D., Le Moine, C., Corvol, J.C., Belluscio, L., Ledent, C., Fienberg, A.A., Jaber, M., Studler, J.M., Girault, J.A., 2001. Galpha(olf) levels are regulated by receptor usage and control dopamine and adenosine action in the striatum. J. Neurosci. 21, 4390–4399.
House, N.C., Koch, M.R., Freudenreich, C.H., 2014. Chromatin modifications and DNA repair: beyond double-strand breaks. Front. Genet. 5, 296.
Jensen, L.J., Kuhn, M., Stark, M., Chaffron, S., Creevey, C., Muller, J., Doerks, T., Julien, P., Roth, A., Simonovic, M., et al., 2009. STRING 8–a global view on proteins and their functional interactions in 630 organisms. Nucleic Acids Res. 37, D412–D416.
Kerrien, S., Alam-Faruque, Y., Aranda, B., Bancarz, I., Bridge, A., Derow, C., Dimmer, E., Feuermann, M., Friedrichsen, A., Huntley, R., et al., 2007. IntAct–open source resource for molecular interaction data. Nucleic Acids Res. 35, D561–D565.
Khan, M.M., Xiao, J., Patel, D., LeDoux, M.S., 2018. DNA damage and neurodegenerative phenotypes in aged Ciz1 null mice. Neurobiol. Aging 62, 180–190.
Kharkwal, G., Brami-Cherrier, K., Lizardi-Ortiz, J.E., Nelson, A.B., Ramos, M., Del Barrio, D., Sulzer, D., Kreitzer, A.C., Borrelli, E., 2016. Parkinsonism driven by antipsychotics originates from dopaminergic control of striatal cholinergic interneurons. Neuron 91, 67–78.
Kim, S.H., Seo, M.S., Jeon, W.J., Yu, H.S., Park, H.G., Jung, G.A., Lee, H.Y., Kang, U.G., Kim, Y.S., 2008. Haloperidol regulates the phosphorylation level of the MEK-ERK-p90RSK signal pathway via protein phosphatase 2A in the rat frontal cortex. Int. J. Neuropsychopharmacol. 11, 509–517.
Kosugi, S., Hasebe, M., Tomita, M., Yanagawa, H., 2009. Systematic identification of cell cycle-dependent yeast nucleocytoplasmic shuttling proteins by prediction of composite motifs. Proc. Natl. Acad. Sci. U. S. A. 106, 10171–10176.
LeDoux, M.S., Dauer, W.T., Warner, T.T., 2013. Emerging common molecular pathways for primary dystonia. Mov. Disord. 28, 968–981.
LeDoux, M.S., Vemula, S.R., Xiao, J., Thompson, M.M., Perlmutter, J.S., Wright, L.J., Jinnah, H.A., Rosen, A.R., Hedera, P., Comella, C.L., et al., 2016. Clinical and genetic features of cervical dystonia in a large multicenter cohort. Neurol. Genet. 2, e69.
Li, J., Guo, Y., Schroeder, F.A., Youngs, R.M., Schmidt, T.W., Ferris, C., Konradi, C., Akbarian, S., 2004. Dopamine D2-like antagonists induce chromatin remodeling in striatal neurons through cyclic AMP-protein kinase A and NMDA receptor signaling. J. Neurochem. 90, 1117–1131.
Liokatis, S., Stutzer, A., Elsasser, S.J., Theillet, F.X., Klingberg, R., van Rossum, B., Schwarzer, D., Allis, C.D., Fischle, W., Selenko, P., 2012. Phosphorylation of histone H3 Ser10 establishes a hierarchy for subsequent intramolecular modification events. Nat. Struct. Mol. Biol. 19, 819–823.
Masuho, I., Fang, M., Geng, C., Zhang, J., Jiang, H., Ozgul, R.K., Yilmaz, D.Y., Yalnizoglu, D., Yuksel, D., Yarrow, A., et al., 2016. Homozygous GNAL mutation associated with familial childhood-onset generalized dystonia. Neurol. Genet. 2, e78.
Matamales, M., Bertran-Gonzalez, J., Salomon, L., Degos, B., Deniau, J.M., Valjent, E., Herve, D., Girault, J.A., 2009. Striatal medium-sized spiny neurons: identification by nuclear staining and study of neuronal subpopulations in BAC transgenic mice. PLoS One 4, e4770.
McVittie, L.D., Ariano, M.A., Sibley, D.R., 1991. Characterization of anti-peptide antibodies for the localization of D2 dopamine receptors in rat striatum. Proc. Natl. Acad. Sci. U. S. A. 88, 1441–1445.
Meyer, E., Carss, K.J., Rankin, J., Nichols, J.M., Grozeva, D., Joseph, A.P., Mencacci, N.E., Papandreou, A., Ng, J., Barral, S., et al., 2017. Mutations in the histone methyltransferase gene KMT2B cause complex early-onset dystonia. Nat. Genet. 49, 223–237.
Morigaki, R., Okita, S., Goto, S., 2017. Dopamine-induced changes in Galphaolf protein levels in striatonigral and striatopallidal medium spiny neurons underlie the genesis of l-DOPA-induced dyskinesia in parkinsonian mice. Front. Cell. Neurosci. 11, 26.
Nair, N., Shoaib, M., Sorensen, C.S., 2017. Chromatin dynamics in genome stability: roles in suppressing endogenous DNA damage and facilitating DNA repair. Int. J. Mol. Sci. 18, E1486.
Nguyen Ba, A.N., Pogoutse, A., Provart, N., Moses, A.M., 2009. NLStradamus: a simple hidden Markov model for nuclear localization signal prediction. BMC Bioinformatics 10, 202.
Nicholas, A.P., Lubin, F.D., Hallett, P.J., Vattem, P., Ravenscroft, P., Bezard, E., Zhou, S., Fox, S.H., Brotchie, J.M., Sweatt, J.D., et al., 2008. Striatal histone modifications in models of levodopa-induced dyskinesia. J. Neurochem. 106, 486–494.
Pan, B., Chen, J., Lian, J., Huang, X.F., Deng, C., 2015. Unique effects of acute aripiprazole treatment on the dopamine D2 receptor downstream cAMP-PKA and Akt-GSK3beta signalling pathways in rats. PLoS One 2015 (10), e0132722.
Pelosi, A., Menardy, F., Popa, D., Girault, J.A., Herve, D., 2017. Heterozygous Gnal mice are a novel animal model with which to study dystonia pathophysiology. J. Neurosci. 37, 6253–6267.
Pozzi, L., Hakansson, K., Usiello, A., Borgkvist, A., Lindskog, M., Greengard, P., Fisone, G., 2003. Opposite regulation by typical and atypical anti-psychotics of ERK1/2, CREB and Elk-1 phosphorylation in mouse dorsal striatum. J. Neurochem. 86, 451–459.
Razin, A., Kantor, B., 2005. DNA methylation in epigenetic control of gene expression. Prog. Mol. Subcell. Biol. 38, 151–167.
Rose, S.J., Yu, X.Y., Heinzer, A.K., Harrast, P., Fan, X., Raike, R.S., Thompson, V.B., Pare, J.F., Weinshenker, D., Smith, Y., et al., 2015. A new knock-in mouse model of l-DOPA-responsive dystonia. Brain 138, 2987–3002.
Salti, A., Kummer, K.K., Sadangi, C., Dechant, G., Saria, A., El Rawas, R., 2015. Social interaction reward decreases p38 activation in the nucleus accumbens shell of rats. Neuropharmacology 99, 510–516.
Sanberg, P.R., Bunsey, M.D., Giordano, M., Norman, A.B., 1988. The catalepsy test: its ups and downs. Behav. Neurosci. 102, 748–759.
Sawicka, A., Seiser, C., 2012. Histone H3 phosphorylation - a versatile chromatin modification for different occasions. Biochimie 94, 2193–2201.
Schar, P., Fritsch, O., 2011. DNA repair and the control of DNA methylation. Prog. Drug Res. 67, 51–68.
Shimizu, S., Tatara, A., Sato, M., Sugiuchi, T., Miyoshi, S., Andatsu, S., Kizu, T., Ohno, Y., 2014. Role of cerebellar dopamine D(3) receptors in modulating exploratory locomotion and cataleptogenicity in rats. Prog. Neuro-Psychopharmacol. Biol. Psychiatry 50, 157–162.
Sibley, D.R., Monsma Jr., F.J., 1992. Molecular biology of dopamine receptors. Trends Pharmacol. Sci. 13, 61–69.
Stark, C., Breitkreutz, B.J., Chatr-Aryamontri, A., Boucher, L., Oughtred, R., Livstone, M.S., Nixon, J., Van Auken, K., Wang, X., Shi, X., et al., 2011. The BioGRID interaction database: 2011 update. Nucleic Acids Res. 39, D698–D704.
Swathy, B., Banerjee, M., 2017. Haloperidol induces pharmacoepigenetic response by modulating miRNA expression, global DNA methylation and expression profiles of methylation maintenance genes and genes involved in neurotransmission in neuronal cells. PLoS One 12, e0184209.
Uhernik, A.L., Li, L., LaVoy, N., Velasquez, M.J., Smith, J.P., 2014. Regulation of monocarboxylic acid transporter-1 by cAMP dependent vesicular trafficking in brain microvascular endothelial cells. PLoS One 9, e85957.
Valjent, E., Bertran-Gonzalez, J., Bowling, H., Lopez, S., Santini, E., Matamales, M., Bonito-Oliva, A., Herve, D., Hoeffer, C., Klann, E., et al., 2011. Haloperidol regulates the state of phosphorylation of ribosomal protein S6 via activation of PKA and phosphorylation of DARPP-32. Neuropsychopharmacology 36, 2561–2570.
Vemula, S.R., Puschmann, A., Xiao, J., Zhao, Y., Rudzinska, M., Frei, K.P., Truong, D.D., Wszolek, Z.K., LeDoux, M.S., 2013. Role of Galpha(olf) in familial and sporadic adult-onset primary dystonia. Hum. Mol. Genet. 22, 2510–2519.
Viyoch, J., Ohdo, S., Yukawa, E., Higuchi, S., 2001. Dosing time-dependent tolerance of catalepsy by repetitive administration of haloperidol in mice. J. Pharmacol. Exp. Ther. 298, 964–969.
Wadenberg, M.L., 1996. Serotonergic mechanisms in neuroleptic-induced catalepsy in the rat. Neurosci. Biobehav. Rev. 20, 325–339.
Wadenberg, M.L., Salmi, P., Jimenez, P., Svensson, T., Ahlenius, S., 1996. Enhancement of antipsychotic-like properties of the dopamine D2 receptor antagonist, raclopride, by the additional treatment with the 5-HT2 receptor blocking agent, ritanserin, in the rat. Eur. Neuropsychopharmacol. 6, 305–310.
Wagner, S.A., Satpathy, S., Beli, P., Choudhary, C., 2016. SPATA2 links CYLD to the TNF-alpha receptor signaling complex and modulates the receptor signaling outcomes. EMBO J. 35, 1868–1884.
Xiao, M.F., Xu, J.C., Tereshchenko, Y., Novak, D., Schachner, M., Kleene, R., 2009. Neural cell adhesion molecule modulates dopaminergic signaling and behavior by regulating dopamine D2 receptor internalization. J. Neurosci. 29, 14752–14763.
Xiao, J., Vemula, S.R., Xue, Y., Khan, M.M., Kuruvilla, K.P., Marquez-Lona, E.M., Cobb, M.R., LeDoux, M.S., 2016. Motor phenotypes and molecular networks associated with germline deficiency of Ciz1. Exp. Neurol. 283, 110–120.
Xiao, J., Vemula, S.R., Xue, Y., Khan, M.M., Carlisle, F.A., Waite, A.J., Blake, D.J., Dragatsis, I., Zhao, Y., LeDoux, M.S., 2017. Role of major and brain-specific Sgce isoforms in the pathogenesis of myoclonus-dystonia syndrome. Neurobiol. Dis. 98, 52–65.
Yokoi, F., Dang, M.T., Li, J., Li, Y., 2006. Myoclonus, motor deficits, alterations in emotional responses and monoamine metabolism in epsilon-sarcoglycan deficient mice. J. Biochem. 140, 141–146.
Zhao, Y., DeCuypere, M., LeDoux, M.S., 2008. Abnormal motor function and dopamine neurotransmission in DYT1 DeltaGAG transgenic mice. Exp. Neurol. 210, 719–730.
Zhou, Z., Ikegaya, Y., Koyama, R., 2019. The astrocytic cAMP pathway in health and disease. Int. J. Mol. Sci. 20, E779.